Redox switching of polyoxometalate-doped polypyrrole films in ionic liquid media

Nargis Anwar, Gordon Armstrong, Fathima Laffir, Calum Dickinson, Mikhail Vagin and Timothy McCormac

Anwar, N., Armstrong, G., Laffir, F., Dickinson, C., Vagin, M., McCormac, T., (2018), Redox switching of polyoxometalate-doped polypyrrole films in ionic liquid media, *Electrochimica Acta*, 265, 254-258.
https://doi.org/10.1016/j.electacta.2017.12.101

Redox switching of polyoxometalate-doped polypyrrole films in ionic liquid media

Nargis Anwar,[a] Gordon Armstrong,[b] Fathima Laffir,[b] Calum Dickinson,[b] Mikhail Vagin*,[c,d] Timothy McCormac[a]

[a]Electrochemistry Research Group, Department of Applied Science, Dundalk Institute of Technology, Dublin Road Dundalk, County Louth, Ireland

[b]Materials and Surface Science Institute, University of Limerick, Limerick, Ireland

[c]Department of Physics, Chemistry and Biology, Linköping University, SE-581 83, Linköping, Sweden;

[d]Laboratory of Organic Electronics, Department of Science and Technology, Linköping University, SE-601 74, Norrköping, Sweden; tel.: +46702753087; mikva@ifm.liu.se

Abstract

The surface immobilization of parent Dawson polyoxometalate (POM) as a counter-ion for electro polymerization of the polypyrrole or as electrode-adhered solid was utilized for the studies of voltammetric responses of POM in environment of room temperature ionic liquids (RTIL). Illustrating the efficiency of intermediate stabilization, voltammetry at POM-modified electrodes in PF_6-based RTIL revealed richer redox behaviour and higher stabilization in comparison with aqueous electrolytes and with BF_4-based RTIL respectively. High stability of POM-doped PPy towards continuous charge-discharge voltammetric cycles was confirmed by minor changes in film morphology observed after the cycling in RTILs.

Keywords: room temperature ionic liquid, polyoxometalate, voltammetry

*Corresponding author

1. Introduction

Ionic liquids are considered as salts with low melting point usually below 100°C and these are generally termed Room Temperature Ionic Liquids (RTIL) {Dupont, 2002 #440;Wasserscheid, 2000 #450;Welton, 1999 #451}. The cationic part of RTIL is usually based on large organic cations such as imidazolium, pyridinium {Welton, 1999 #451}, pyrrolidinium{MacFarlane, 1999 #452} and phosphonium ions{Chen, 2002 #441}, while the combination of different anionic parts like chloride and bromide or fluorine based anions (i.e. hexafluorophosphate) to these large cations give them their hydrophilic or hydrophobic properties respectively {Binnemans, 2007 #424;Welton, 1999 #451}. High thermal stability, low volatility, high ionic conductivity and an wide electrochemical window are among the attractive properties shown by RTIL {Brennecke, 2001 #447;Li, 2005 #432}. This makes them highly attractive for application in catalysis, synthesis of new materials and separation processes {Brennecke, 2001 #447;Endres, 2006 #427;Seddon, 1997 #454;Welton, 2004 #433;Zhao, 2002 #444}. The variety of physicochemical properties of ionic liquids such as miscibility with solvents, viscosity, polarity and density can be tuned by the selection of the cationic and the anionic moieties, which enhances the desired properties of RTIL {Binnemans, 2007 #424}.

Tungsten, vanadium, molybdenum, niobium and tantalum belong to the early transition metals and are capable of making metal-oxide cluster anions in their highest oxidation state. These anions are generally referred as polyoxoanions or polyoxometalates (POM). The building blocks of these large anions are consisted of tetrahedrally bonded MO_6 units, where M represents the transition metals atoms {Pope, 1983 #1}. Since the first discovery of POM around 200 years ago, novel structures are being synthesized continuously. The diversity in their molecular and electronic structures enabled them to be used across the wide range of applications from molecular electronics to medicine and catalysis {Pope, 1991 #2}.

Produced by pairing with organic cations or RTIL, POM-based hybrid materials have been recently studied and exhibited a range of exciting physicochemical properties such as photochromism {Gamelas, 2002 #439;Huang, 2006 #426}, catalysis {Vazylyev, 2005 #430}, proton conduction {Stangar, 2001 #446} etc. New challenges are addressed regarding catalytic and electrochemical properties of these materials {Kim, 2007 #423;Leng, 2009 #418;Mioc, 2005 #428}. The improvement of POM's electrochemical responses by using RTIL either as solvent or as a modifier to develop POM-modified electrodes {Ammam, 2011 #415;Chiang,

2004 #434;Goral, 2009 #419;Haghighi, 2009 #417;Rajkumar, 2008 #421;Rao, 2009 #420;Wang, 2009 #416;Zhang, 2005 #429}.

Due to the delocalisation of electrons within the conjugated structure of the backbone, conducting polymers valuably combine the mechanical flexibility and lightness of the polymers with the electronic properties of metals. Among the variety of conducting polymers, polypyrrole (PPy) is highly conductive and easily synthesizable, which makes PPy attractive for the range of applications such as light emitting diodes {Shen, 1998 #453}, sensing {Bhat, 2003 #438;Ramanaviciene, 2002 #445}, battery systems {Levi, 2002 #442} and the electromechanical actuators {Baughman, 1996 #455}. POM have been used as dopant anions during the polymerisation of PPy {Anwar, 2012 #295;Bidan, 1989 #25} maintaining the inherent electrochemical properties after the incorporation into the conducting polymer. However, the main focus of these studies was confined to the aqueous media. Showing a multiple redox processes in RTIL due to the metal-oxide framework {Goral, 2009 #419}, POM are the attractive materials for fuel cells, batteries or molecular electronics.

Here we report the comparative study of the redox phenomena of parent Dawson POM in RTILs media with the attachment to the electrode surface via the conducting polymer entrapment or the surface-immobilized solids.

2. Experimental

2.1 Materials

1-n-butyl-3-methylimidazoilium tetrafluroborat (termed as BMIM-BF_4), 1-n-butyl-3-methylimidazoilium hexaflurophosphate (termed as BMIM-PF_6), 1-n-butyl-3-methylimidazoilium bromide (termed as BMIM-Br) and all other chemicals were purchased from Sigma-Aldrich and were used as received unless otherwise stated. The parent Dawson POM α_2–$K_6[P_2W_{18}O_{62}]\cdot 14H_2O$ was synthesised and characterised as described in the literature [REF]. The 1-n-butyl-3-methylimidazoilium salt of POM ($(BMIM)_6[P_2W_{18}O_{62}]$ (termed as BMIM-POM)) was synthesised by extracting the method from the literature {Rajkumar, 2008 #421}. Pyrrole (99%) was received from ACROS Organics and purified before use by passing through a neutral Al_2O_3 column to obtain a colourless liquid. Alumina powders of sizes 0.05, 0.3 and 1.0 μm were received from CHI Instruments. Water was purified using a Milli-Q water purification system.

2.2 Apparatus and Procedures

2.2.1 Electrochemical measurements

All electrochemical experiments were performed with a CHI660 electrochemical work station in a conventional three-electrode electrochemical cell using a glassy carbon electrode (GCE, 3mm diameter) as the working electrode, a platinum wire as the auxiliary electrode. A silver/silver chloride reference electrode (3M KCl) was used for the experiments in the aqueous media. A platinum wire was used as the pseudo-reference electrode in the measurements in RTIL. Having a fast and reversible one electron redox process at the electrode material-independent half wave potential, ferrocenium/ferrocene redox couple (Fc/Fc^{+}) has been used as the reference standard {Gritzner, 1984 #457;Stojanovic, 1993 #456} in order to address the observed electrochemical processes in RTIL {Hultgren, 2002 #443}.

Prior to use the GCE was polished with 1.0, 0.3 and 0.05 μm Al_2O_3 powders, successively, and sonicated in water for about 10 min after each polishing step. Finally, the electrode was sonicated and washed with ethanol, then dried with a high purity nitrogen stream immediately before use. RTIL were degassed for at least 20 min with high-purity nitrogen and kept under a blanket of nitrogen during all electrochemical experiments.

2.2.2 Electrode modifications

The water solution of POM was drop-casted onto the surface of GCE. The dried film-modified electrode was used as a working electrode for the voltammetry measurements with surface-adhered crystals of POM.

Electrosynthesis of PPy in the presence of POM as a counter-ions was utilized for the electrode surface modification {Anwar, 2012 #295;Bidan, 1989 #25;McCormac, 2001 #103}. Films of different thicknesses were grown by chronocolometry (charges up to 1 mM, 5 mC and 10mC at +0.65 V) or by cyclic voltammetry (from +0.7 V to -0.5 V, 5 or 10 cycles, 40 mV s^{-1}) in a 0.1 M pyrrole and 5 mM POM in water.

2.2.3 X-ray photoelectron spectroscopy (XPS)

POM-doped and RTIL-doped polymer films deposited on ITO glass slides were characterised with XPS. Analysis was performed in a Kratos AXIS 165 spectrometer using monochromatic Al Kα radiation of energy 1486.6 eV. High resolution spectra were taken at a fixed pass energy of 20 eV. In the near-surface region the atomic concentrations of the chemical elements were evaluated after subtraction of a Shirley type background by considering the corresponding Scofield atomic sensitivity factors. Surface charge was efficiently neutralised by flooding the sample surface with low energy electrons. Core level binding energies were determined using

C 1s peak at 284.8 eV as the charge reference.

2.2.4 Scanning Electron Microscopy (SEM)

SEM of the films was performed on a Hitachi SU-70 FESEM using accelerating voltages of 3 kV and 20 kV. Films were deposited onto ITO coated glass slides for recording the SEM images. Films were uncoated as a low voltage (3kV) was employed to avoid charging effects during imaging. Energy Dispersive Spectroscopy (EDS) used an Oxford Instruments SDD X-max detector with 50 mm^2 window and operated at accelerating voltage of 20 kV.

2.2.5 Atomic Force Microscopy (AFM)

AFM was conducted in AC ('tapping') mode on an Agilent 5500 controlled using PicoView 1.10.1 software. Micromasch NSC15 or Olympus AC 160 TS cantilevers having tetrahedral tips of radius < 10 nm with a resonant frequency of 325 KHz or 300 KHz, respectively, were used. The areas of interest examined and image sizes used for each sample were chosen based on the expected dimensions of the features of interest identified from SEM analysis. Multiple areas were imaged on each sample to ensure that the high resolution images presented here were representative of the entire sample. Scan speeds were optimized to suit the features observed for each sample.All images presented were obtained at 512 pixel resolution. Image analysis was undertaken using PicoImage Advanced 5.1.1 software. The raw topography and amplitude data was leveled, noise was removed by applying a spatial filter, and line noise arising from artefacts was removed where necessary. Height parameters for each sample were determined according to ISO 25178. The resulting topography and amplitude profiles are presented as pseudo-colour images.

3. Results and Discussion

3.1 Redox processes of POM and its BMIM derivative in contact with RTILs

As soon as adhered solid starts to dissolve into the ionic liquid during the first voltammetry scan, the presented cyclic voltammogram of electrode modified by POM in BMIM-BF_4 is solution-based data (Fig. 1A). The procedure of solid POM attachment allows to avoid the interfering impurities which could appear in the solution during prolonged periods of exposures of POM in RTIL {Zhang, 2005 #429}. The six well-defined reversible one electron redox processes associated with the W-O framework of the POM are clearly seen, which can be presented by a sequence of the following six redox processes:

$$[P_2W_{18}O_{62}]^{6-} + 1e \Leftrightarrow [P_2W_{18}O_{62}]^{7-} + 1e \Leftrightarrow [P_2W_{18}O_{62}]^{8-} + 1e \Leftrightarrow [P_2W_{18}O_{62}]^{9-} + 1e \Leftrightarrow$$
$$[P_2W_{18}O_{62}]^{10-} + 1e \Leftrightarrow [P_2W_{18}O_{62}]^{11-} + 1e \Leftrightarrow [P_2W_{18}O_{62}]^{12-} \quad (1)$$

The redox phenomena of parent Dawson POM in aqueous solutions are characterized with two bi-electronic transfers followed by two mono-electronic processes {Anwar, 2012 #295}. The difference of POM redox processes in RTIL illustrates a higher ability of the medium for intermediates solvation and stabilization.

The values for the peak-to-peak separations (ΔE_p) for these six redox processes are within the range of 76 ± 10 mV, which is close to ΔE_p for the standard reversible mono-electronic redox couple Fc^+/Fc in the same medium (78mV). The redox processes were found to be stable between scan rates 10-100mV/s within the chosen potential window. A gaps of 250-300 mV are visible between the redox processes 1 - 2, 3 - 4 and 5 - 6, whereas a gaps of almost 350-450 mV were observed between the processes 2 - 3 and 4 - 5, which is in good agreement with the literature {Zhang, 2005 #429}.The formal potentials for each of these redox processes are summarised in Table 1S.

The voltammetric response of POM in BMIM- PF_6 (Fig. 1B) exhibits four well-defined mono-electronic redox processes (1-4), whereas the subsequent two redox processes (5 and 6) are characterized with poor-defined peak couples. The cathodic shift of approximately 200mV is observed for all redox processes in comparison with the voltammetric responses observed in BMIM-BF_4. The values of ΔE_p for the first four mono-electronic redox couples were in the range of 75 ± 10 mV, which is again close to the standard Fc^+/Fc couple in the same medium. Attributed with the peak broadening, the processes 5 and 6 are characterized with larger ΔE_p (108 mV and 159 mV respectively), which probably illustrates the impact of high uncompensated resistance {Sukardi, 2008 #422}. The formal potentials for each of these redox processes are summarised in Table 1S and are in close agreement with the literature {Bernardini, 2011 #414}.

The counter-ion substitution by the cation of RTIL led to the appearance of the whole set of mono-electronic redox processes of POM (Fig. 1C and 1D), illustrating the better intermediate stabilization by the substituted compound. The observed voltammetric responses are characterized with the same parameters obtained for POM in BMIM-BF_4.

3.2 Redox switching of POM-doped PPy films in RTIL

As it was observed previously, the use of RTIL as an electrolyte and as a doping agent leads to the enhancement of degree of conducting polymer doping {Pringle, 2004 #435}. PPy was

chosen as the supporting conductive matrix for the surface attachment of POM. Static and dynamic regimes of applied potential control (i.e. cyclic voltammetry and chronocoulometry, respectively) were used for the polymerization of PPy in aqueous media in a presence of POM as a counter-ion yielding the fabrication of POM-doped PPy films. The number of cycles or the elapsed charge allowed the control of amount of polymerized material.

The effect of solvent anion is visible as a difference in the redox behaviour of electrodes modified by POM-doped PPy obtained in BF_4- and in PF_6-based TRILs. In contrast to adherent solid-modified electrode, the film-modified electrodes fabricated by both static and dynamic regimes showed only four redox couples associated with the W-O framework of POM in BMIM-BF_4 (Fig. 2A). The extension of voltammetric window towards more cathodic potentials did not show any additional redox peaks. The increase of capacitive currents at the anodic limit of voltammetry illustrates the transition between insulating (i.e. at -2V) and conductive (i.e. at 0V) states of PPy (Fig. 1SA). Thus, only the first redox process of W-O network observed in BMIM-BF_4 is within the conducting domain of PPy. The film fabricated via dynamic growth (dashed curve at Fig. 2A) reveals four well-defined redox couples with cathodic shift of 60 mV with respect to the peaks of film fabricated by static growth. The formal potentials of redox processes of POM-doped PPy films have a cathodic shifts of ca. 300 mV in comparison with the formal redox potentials for adhered solid POM observed in the same RTIL illustrating the change of the environment of POM due to the immobilization within the PPy matrix. The decrease of ΔE_p due to the immobilization within PPy observed for all redox processes illustrates the surface-confined redox behaviour, which was confirmed by the scan rate study up to 75 mV s^{-1}.

The surface coverage of the films was estimated employing $\Gamma = Q/nFA$, where Q is the integrated charge (C) of first redox process of the film and measured at slow scan rate; n is the number of transferred electrons for this redox process, which is equal to 1 for the W-O framework; F is Faraday's constant (96,485 C mol^{-1}) and A is the electrode surface area (0.0707 cm^2). The values for the film's surface coverage as a function of layer number showed a continuous film growth for the multilayer film. The resulting surface coverage values for the films were found to be in the range of 3.5 - 23.1 nmol·cm^{-2}, which is typical for films of conducting polymers.

Visible change of voltammetric response was observed in BMIM-PF_6 (Fig. 2B and 2C) in comparison with BMIM-BF_4 illustrating the effect of the RTIL anion. Six well-defined mono-electronic redox couples of W-O framework were clearly observed at the potentials close to

the observed for adherent solid POM in the same RTIL. The location of first and second redox processes of POM within the conducting region of PPy (Fig. 1SB) probably led to the faster kinetics of electron transfer in contrast to the rest of the couples appeared in the insulating region of polymer and characterized with slower kinetics and higher peak-to-peak separation. The surface-confined redox processes were attributed by the decrease of peak-to-peak separation, which was confirmed by the scan rate studies up to 100 mV s^{-1}. Potentiodynamic growth led to the formation of POM-doped PPy films of higher amount of entrapped dopant, as it seen from higher peak currents of W-O redox processes accompanied with minor changes in PPy capacitive currents.

Section on film stability and linking to energy storage needs to here

3.3 Surface analysis of POM-doped PPy films

Surface composition of deposited films were determined by XPS on ITO glass slides coated with POM- or RTIL-doped PPy. The high resolution C 1s and N 1s spectra (Fig. 2S) confirm the presence of PPy. The C 1s spectra can be decomposed into two major peaks to represent C-C/C=C at 284.8 eV and C-N of the PPy chains at 286 eV, and two minor peaks at 287.5 and 289 eV to represent oxidised carbon. The N 1s spectra can be decomposed mainly into 2 component peaks. The lower binding energy peak at 399.9 eV is attributed to neutral nitrogen in PPy and the peak at binding energy greater than 401 eV is attributed to protonated nitrogen. The ratio of N^{+}/N(total) for $[P_2W_{18}O_{62}]^{6-}$-, $BF_4^{1-}$and PF_6^{1-}doped polymer are 0.26, 0.76 and 0.16 respectively and could give an estimate of the doping levels. The presence of the POM dopant is evident from the presence of W, O and P and in the case of BF_4- and PF_6-doped PPy films, presence of F and the absence of W.

The SEM images of POM-doped PPy films obtained before (Fig. 3A) and after (Fig. 3B) voltammetric cycling in BMIM-PF_6 reveal minor change in morphology illustrating a good stability of developed electrode material. The films are characterized with the presence of large connected particles (400-500 nm). Small particles, < 50 nm, could also be seen decorating the surface of the larger particles. Some micron sized circular islands of the films can still be seen formed by similar sized particles. EDX results of the same films also confirmed the elements present and showed the presence of W, C, N and O, which is in good agreement with the XPS results. The presence of tungsten, does indicate that the POM is present.

Consistent with the SEM results, AFM imaging (Fig. 3C and 3D) did not show any significant impact of voltammetric cycling onto the topography of the POM-doped PPy films confirning

a good operation stability of the material. The globular structures were observed by AFM; the diameter of these globules as well as film thickness varied significantly by the growth conditions. The observed little phase contrast sugests a presence of the homogenous polymer film within the areas of interest imaged.

4. Conclusions:

The entrapment within the conducting polymer and the surface attachment of solids were utilized for the electrochemical studies of POM and its BMIM derivative in RTILs. Voltammetry at modified electrodes revealed richer redox behaviour in comparison with aqueous electrolytes due to the higher efficiency of intermediate stabilization in RTIL media. The effect of RTIL anion has been observed at POM-doped PPy films developed by both static and dynamic regimes of applied potential control. In contrast to BF_4 anion, the voltammetric response of POM-doped PPy in PF_6-based RTIL showed six consequtivre redox processes illustrating higher efficiency of intermediate stabilization. High stability of POM-doped PPy towards continuous charging-discharging was confirmed by minor changes in film morphology observed after the cycling in RTILs.

References

Figure Legends

Figure 1. Effect of substitution of counter-ion. Cyclic voltammograms were recorded in BMIM-BF_4 (**blue curves**) and in BMIM-PF_6 (**magenta curves**) at GCE electrodes modified with adherent POM (**A** and **B**) and BMIM-POM (**C** and **D**); 10 mV s^{-1}.

Figure 2. Effects of RTIL anion and regimes of electropolymerization. Cyclic voltammograms recorded in BMIM-BF4 (**A**) and in BMIM-PF_6 (**B** and **C**) at electrodes modified with POM-doped PPy films fabricated by different regimes. **A:** films fabricated by static (3.5 nmol cm^{-2}, solid line) and dynamic (6.6 nmol cm^{-2}, dashed line) regimes; **B:** films fabricated by dynamic regime (5 cycles (0.4 nmol cm^{-2}) and 10 cycles (0.8 nmol cm^{-2}) dashed and solid lines, respectively); **C:** films fabricated by static regime (1, 5 and 10 mC (black, red and blue lines, respectively)). 100 mV s^{-1}.

Figure 3. The minor changes of morphology of polymer with voltammetric cycling. SEM (**A** and **B**) and AFM images (**C** and **D**) of the POM-doped PPy films on ITO glass slide before (**A** and **C**) and after (**B** and **D**) cycling in BMIM- PF_6.

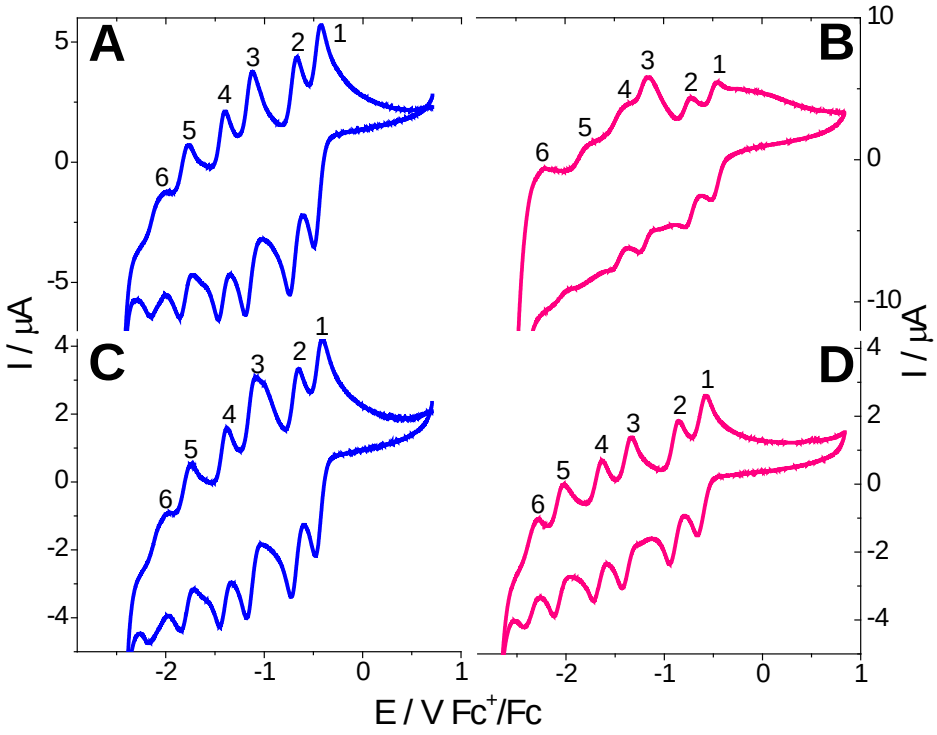

Figure 1.

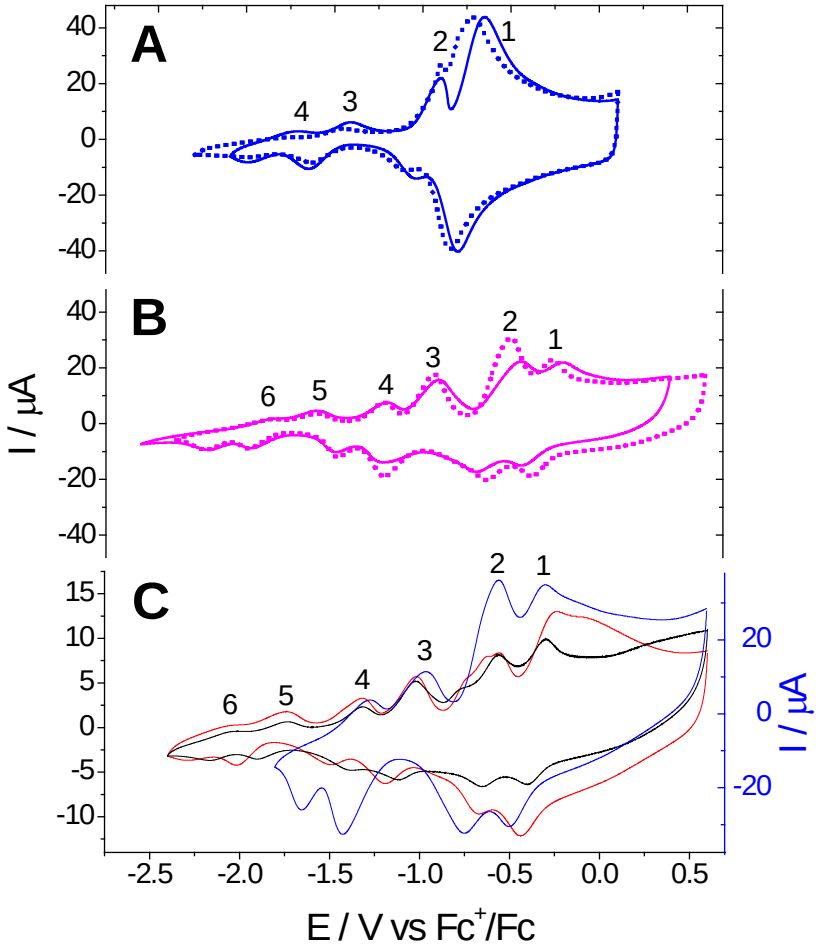

Figure 2.

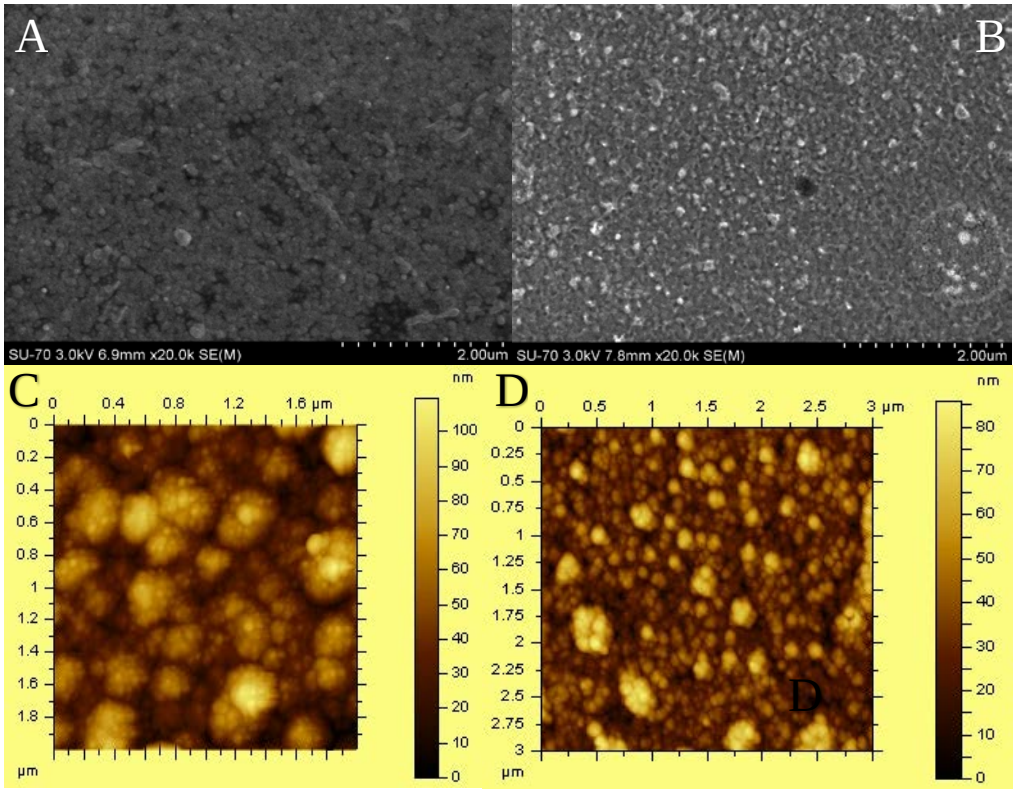
A
B
SU-70 3.0kV 6.9mm x20.0k SE(M)
2.00um
SU-70 3.0kV 7.8mm x20.0k SE(M)
2.00um
C
D
nm
µm

Figure 3.